Negative anisotropic magnetoresistance resulting from minority spin transport in $Ni_XFe_{4-X}N$ (x = 1 and 3) epitaxial films

Fumiya Takata, Kazuki Kabara, Keita Ito, Masakiyo Tsunoda, and Takashi Suemasu

Citation: Journal of Applied Physics **121**, 023903 (2017); doi: 10.1063/1.4974002
View online: http://dx.doi.org/10.1063/1.4974002
View Table of Contents: http://aip.scitation.org/toc/jap/121/2
Published by the American Institute of Physics

Negative anisotropic magnetoresistance resulting from minority spin transport in $Ni_xFe_{4-x}N$ ($x = 1$ and 3) epitaxial films

Fumiya Takata,[1] Kazuki Kabara,[2] Keita Ito,[1,2,3,a)] Masakiyo Tsunoda,[2] and Takashi Suemasu[1]

[1]*Institute of Applied Physics, Graduate School of Pure and Applied Sciences, University of Tsukuba, Tsukuba, Ibaraki 305-8573, Japan*

[2]*Department of Electronic Engineering, Graduate School of Engineering, Tohoku University, Sendai 980-8579, Japan*

[3]*Japan Society for the Promotion of Science (JSPS), Chiyoda, Tokyo 102-0083, Japan*

(Received 25 October 2016; accepted 31 December 2016; published online 12 January 2017)

We grew 50 nm-thick $Ni_xFe_{4-x}N$ ($x = 1$ and 3) epitaxial films on a $SrTiO_3$(001) single-crystal substrate by molecular beam epitaxy and measured their anisotropic magnetoresistance (AMR) ratios r_{AMR} in the temperature range of 5–300 K with current directions set along either $Ni_xFe_{4-x}N$ [100] or [110]. A negative r_{AMR} was obtained up to 200 K or higher. Their magnitude $|r_{AMR}|$ increased with decreasing temperature. From the negative AMR effect and the negative spin-polarization of density of states for $Ni_xFe_{4-x}N$ at the Fermi level, it can be stated that the minority spin transport is dominant in $Ni_xFe_{4-x}N$, similar to Fe_4N and Co_3FeN. The r_{AMR} depends on the current direction that arises from the current direction dependence of *s-d* scattering. In the case of Ni_3FeN, the r_{AMR} decreased to nearly zero at 260 K. This temperature agreed well with the Curie temperature determined from the temperature dependence of magnetization. The AMR curves were reproduced well by using both $\cos2\phi$ and $\cos4\phi$ components below 100 K, whereas a $\cos2\phi$ component was enough to fit those obtained above 100 K. It is assumed that the tetragonal crystal field was enhanced at low temperatures (<100 K) similar to Fe_4N (<50 K). *Published by AIP Publishing.*
[http://dx.doi.org/10.1063/1.4974002]

I. INTRODUCTION

Ferromagnetic materials with a high spin-polarization can actualize spin dependent transport phenomena such as giant magnetoresistance effect and tunneling magnetoresistance (TMR) effect. Ferromagnetic nitride Fe_4N, which has an anti-perovskite cubic crystal structure, is theoretically predicted to have a negative spin polarization of the density of states (D) at the Fermi level (E_F), P_D, and a very large negative spin-polarization of the electrical conductivity $P_\sigma = -1.0$.[1] Thereby, a highly spin-polarized electrical current due to minority spins is anticipated in Fe_4N. The high spin-polarization in Fe_4N was experimentally confirmed via point-contact Andreev reflection ($|P_\sigma| = 0.59$).[2] It is considered that the inverse TMR effect and inverse current-induced magnetization switching effect in Fe_4N/MgO/CoFeB magnetic tunnel junctions are caused by the minority spin transport in Fe_4N.[3–6]

Recently, several studies on magnetotransport properties in ferromagnetic materials such as anisotropic magnetoresistance (AMR) effect have been conducted theoretically[7–9] and experimentally.[10–20] Kokado *et al.* derived a general expression of the AMR ratio r_{AMR} from the two-current model, which consists of a spin-polarized conduction state and localized *d* states with spin-orbit interaction (SOI). They used a resistivity of the conduction state and resistivities due to *s-d* scattering processes from the conduction state to the localized *d* states, and expressed r_{AMR} as[7]

$$r_{AMR} = \frac{\rho_{\parallel} - \rho_{\perp}}{\rho_{\perp}} \propto -\gamma \cdot \left[D_{\uparrow}^{(d)} - D_{\downarrow}^{(d)}\right] \cdot (\sigma_{\uparrow} - \sigma_{\downarrow}), \quad (1)$$

with $\gamma = (3/4)(\lambda/H_{ex})^2$. Here, λ is the spin-orbit coupling constant, and H_{ex} is the exchange field. $\rho_{//}[\rho_{\perp}]$ represents the resistivity when the magnetization (M) is parallel [perpendicular] to the electrical current (I). $D_{\uparrow}^{(d)}[D_{\downarrow}^{(d)}]$ is the majority (↑) [minority (↓)] D for 3*d* electrons at E_F. In addition, $\sigma_{\uparrow}[\sigma_{\downarrow}]$ is the electrical conductivity for majority [minority] electrons. In a 3*d* transition ferromagnetic metal, the 3*d* electrons are dominant in the D at E_F. Hence, the sign of $[D_{\uparrow}^{(d)} - D_{\downarrow}^{(d)}]$ is the same as that of P_D. Equation (1) means that the sign of P_σ, thereby, the sign of $(\sigma_{\uparrow} - \sigma_{\downarrow})$, is determined by those of r_{AMR} and P_D. In accordance with this expression, the fact that the minority spins dominate the electrical conductivity in Fe_4N was confirmed by the negative r_{AMR}.[10–15] In the same manner, the negative r_{AMR} in Co_3FeN indicates that the minority-spin electrons determine the electrical conductivity.[14]

$Ni_xFe_{4-x}N$, which has the same crystal structure as Fe_4N, is predicted to have a larger P_D of −0.86 than Fe_4N ($P_D = -0.49$) when $x = 3$ (Ni_3FeN). Thereby, it is a candidate material for a highly spin-polarized electron source.[21] Previously, we successfully grew $Ni_xFe_{4-x}N$ ($x = 0$, 1, 3, and 4) films by molecular beam epitaxy (MBE) and investigated their magnetic properties.[21] The Curie temperature (T_c) of Ni_3FeN was found to be lower than 300 K. According to Loloee, however, Ni_3FeN epitaxial films grown on an Al_2O_3(11–20) substrate exhibited a large positive r_{AMR} reaching 6% at room temperature (RT).[22] This result means that the T_c of Ni_3FeN was above RT in contrast to our result.

a)Present address: Institute for Materials Research, Tohoku University, Sendai 980-8577, Japan. Electronic mail: itok@imr.tohoku.ac.jp

Therefore, a question as to why such a positive large r_{AMR} was obtained at RT arises. In this study, we measured the r_{AMR} of $Ni_xFe_{4-x}N$ ($x=1$ and 3) films grown on a $SrTiO_3$ (STO)(001) single-crystal substrate and investigated their sign and magnetotransport properties.

II. EXPERIMENT

50 nm-thick $Ni_xFe_{4-x}N$ ($x=1$ and 3) films were grown on STO(001) single-crystal substrates by MBE using solid sources of Ni and Fe and radio-frequency (RF) N plasma at a substrate temperature $T_S=550\,^{\circ}C$ for $x=1$ and $T_S=300\,^{\circ}C$ for $x=3$. The RF plasma power was set to 105 W, and the Ni/Fe ratio was controlled by their crucible temperatures. After growth, a 3 nm-thick Al capping layer was deposited *in situ* to prevent oxidation of the grown layers. The crystalline quality of grown films was evaluated by reflection high-energy electron diffraction (RHEED) observed along the STO[100] axis, out-of-plane ($\omega-2\theta$) x-ray diffraction (XRD), and in-plane ($\varphi-2\theta_\chi$) XRD measurements with Cu-$K\alpha$ radiation. The occupation probability of N site, the degree of order (S), was calculated from the integrated intensities of the fundamental $Ni_xFe_{4-x}N(200)$ and super lattice $Ni_xFe_{4-x}N(100)$ peaks from XRD patterns.[13,23] Calculation details are described in our previous paper.[21] We assumed that Ni and Fe atoms were randomly distributed in the lattice. The resistivity of the films was measured from 8 to 300 K by van der Pauw method using a closed-cycle He cryostat. A photolithographic process and Ar ion milling were used to pattern the films into stripes with a width of 0.2 mm and a length of 6 mm for AMR measurement. The stripes were patterned along either the $Ni_xFe_{4-x}N[100]$ or [110] direction. The AMR measurements were performed using Quantum Design Physical Property Measurement System equipped with a motorized sample rotator in the temperature range of 5–300 K, by a DC four-probe method with the external magnetic field (H) of 30 kOe, and the current I of 0.2 mA along the stripes. The relative angle ϕ between H and I was changed from 0° to 360°, and the ϕ dependence of resistivity $\rho(\phi)$ was measured. The direction of M corresponds to that of H because the magnitude of H was sufficiently large to saturate the magnetization of samples.

III. RESULT AND DISCUSSION

Figures 1 and 2 show out-of-plane and in-plane XRD patterns of the samples, respectively. The c-axis oriented diffraction peaks corresponding to nitrides were observed in each composition, indicating that single-phase nitride was epitaxially grown on the STO(001) substrate. The S values were calculated to be 0.83 for $x=1$ and 0.72 for $x=3$.

Figure 3 shows the temperature dependence of the resistivity of $Ni_xFe_{4-x}N$ ($x=1$ and 3) films. A gradual decrease in resistivity with decreasing temperature indicates that no structural transformation occurs in the samples.[11] The resistivity began to saturate at a low temperature region (<50 K) and this tendency was observed in Fe_4N, too.[10–14] The resistivities were 38 and 45 $\mu\Omega$ cm at 8 K, and increased up to 101 and 105 $\mu\Omega$ cm at 300 K for $x=1$ and 3, respectively. These

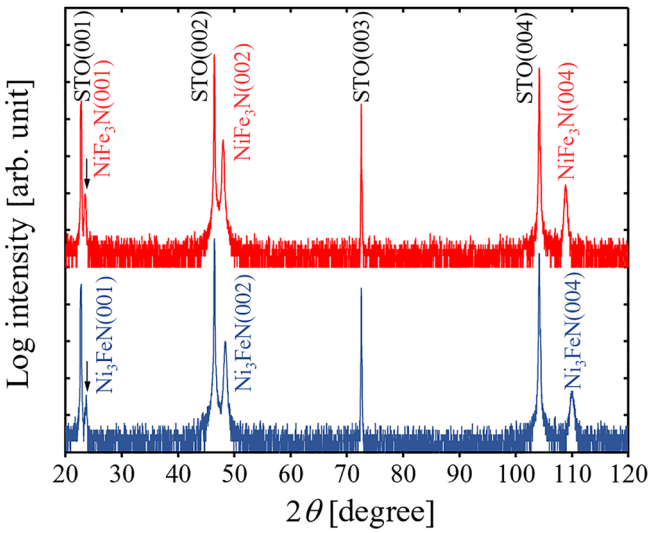

FIG. 1. Semi-logarithmic plots of out-of-plane XRD patterns of $NiFe_3N$ and Ni_3FeN films.

values were larger than those of pure metals (Ni_xFe_{4-x})[24] as well as other nitrides such as Fe_4N, Co_3FeN, and Co_4N.[10–14]

Figure 4 shows the AMR curves of $NiFe_3N$ film with I set along the (a) [100] and (b) [110] axes of the epitaxial layer, which are the angular dependences of resistivity change $[\rho(\phi)-\rho_\perp]$ normalized by $\rho_\perp$. At $\phi=0°$ and 180°, the measured values are equal to r_{AMR}. The AMR curves were composed of cosine functions. The negative AMR effects were observed up to 200 K with I || $NiFe_3N[100]$ and 250 K with I || $NiFe_3N[110]$. Their magnitudes were increased with decreasing temperature. At higher temperatures, the sign of r_{AMR} was positive. The sign change of r_{AMR} cannot be explained by s-d scattering theory described by Eq. (1). As discussed later, the crystal field effect should be taken into consideration for this change.[9]

Figure 5 shows the AMR curves of Ni_3FeN. Negative r_{AMR} was also confirmed up to 260 K, and their magnitude

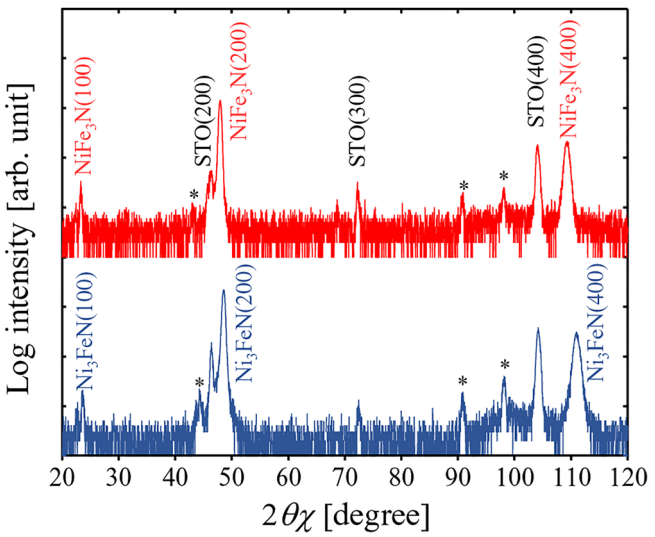

FIG. 2. Semi-logarithmic plots of in-plane XRD patterns of $NiFe_3N$ and Ni_3FeN films. The peak labeled with an asterisk indicates the diffractions caused by the Cu-$K\beta$ or W-$L\alpha$ x-rays.

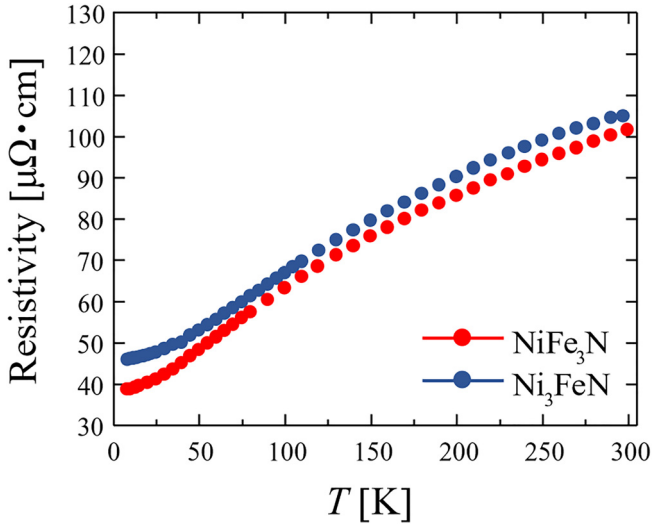

FIG. 3. Resistivities of $NiFe_3N$ and Ni_3FeN films as a function of temperature.

was increased as the measurement temperature decreased. Above 260 K, the AMR curves did not show any ϕ dependence. The T_c of Ni_3FeN was determined to be about 260 K from the temperature dependence of magnetization.[21] This might be the reason why r_{AMR} is close to 0 at 250 K or higher in Figs. 5(a) and 5(b). Although the AMR curves were fitted well by using cosine functions, some anomalies shown by arrows in Fig. 5(a) appeared when we set the I along the [100] axis of Ni_3FeN. We discuss this origin later. Here, we explore the reason why our result ($r_{AMR} < 0$) is different from that reported previously ($r_{AMR} > 0$).[22] NiFe alloys exhibit an r_{AMR} larger than typical ferromagnets such as bcc-Fe, fcc-Ni, and fcc-Co, and the r_{AMR} of Ni_3Fe reaches 3% at RT and exceeds 10% at 14 K.[25,26] In the case of Ni_3FeN, however, the r_{AMR} is negative and its magnitude is 4% at most even at 5 K as shown in Figs. 5(a) and 5(b). We therefore suspect that such a large positive r_{AMR} at RT in Ref. 22 is attributed to N-lacking Ni_3FeN, namely, Ni_3Fe. This assumption is supported in the following way. In

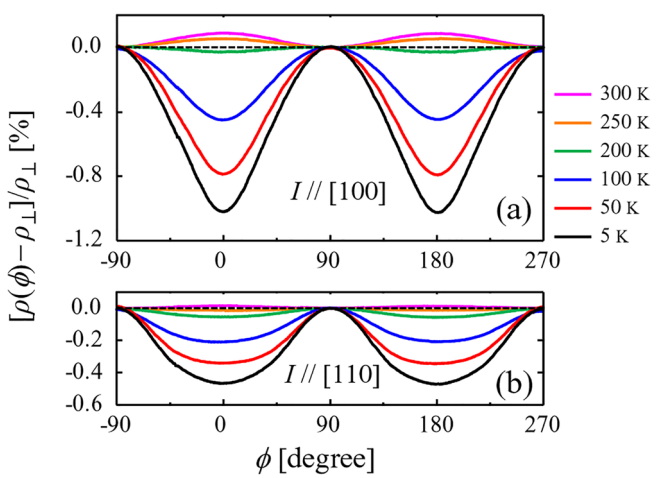

FIG. 4. $[\rho(\phi) - \rho_\perp]/\rho_\perp$ curves of $NiFe_3N$ films measured at temperatures from 5 to 300 K. I was set along the (a)[100] and (b)[110] axes of the epitaxial films.

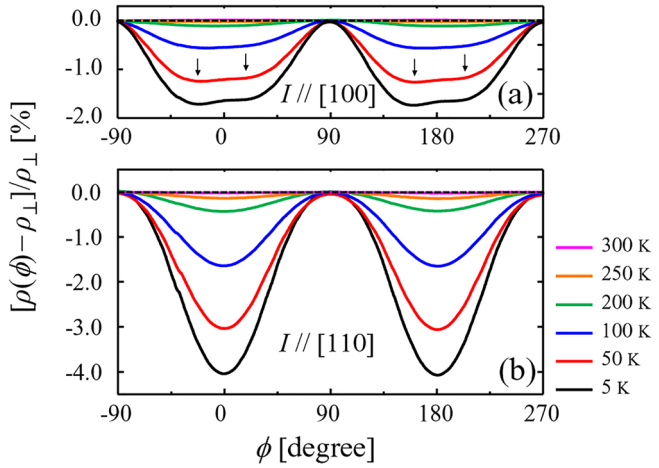

FIG. 5. $[\rho(\phi) - \rho_\perp]/\rho_\perp$ curves of Ni_3FeN films measured at temperatures from 5 to 300 K. I was aligned along the (a)[100] and (b)[110] axes of the epitaxial films.

Ref. 22, T_c was 883 K and the saturation magnetization (M_s) was 900 emu/cm^3 at RT. These values are actually close to those of Ni_3Fe,[24] and so different from our results: $T_c \sim 260$ K and $M_s = 480$ emu/cm^3 at 2 K.[21] Furthermore, Ni_3FeN easily releases N atoms and begins to decompose at $T_S = 400\,^\circ$C or higher,[21] whereas Ni_3FeN was grown at $T_S = 450\,^\circ$C in Ref. 22. Besides, a lattice constant $a = 0.351$ nm, deduced from the XRD peak position $2\theta = 52^\circ$ ascribed to $Ni_3FeN(002)$ in Ref. 22, is close to $a = 0.355$ nm for Ni_3Fe, contrary to our result of $a = 0.376$ nm ($2\theta = 48.4^\circ$). On the basis of these discussions, we may state that N was deficient or completely missing in the measured sample in Ref. 22; thus, Ni_3Fe was formed rather than Ni_3FeN, resulting in a positive r_{AMR}.

We next deduce the sign of P_σ using Eq. (1). From $r_{AMR} < 0$ shown in Figs. 4 and 5, and aforementioned theory stating $P_D < 0$,[21] the relation of $(\sigma_\uparrow - \sigma_\downarrow) < 0$ is obtained from Eq. (1). We therefore can state that the minority spin conduction is dominant in these materials at least in the temperature range of $r_{AMR} < 0$. These magnetotransport properties are similar to those in Fe_4N and Co_3FeN.[10–15]

The temperature dependence of r_{AMR} of $Ni_xFe_{4-x}N$ ($x = 1$ and 3) films with $I \parallel [100]$ and [110] are shown in Fig. 6. The $|r_{AMR}|$ was gradually increased with decreasing temperature and significantly increased below 100 K. The r_{AMR} of $NiFe_3N$ (Ni_3FeN) reached a minima of -1.0% (-1.6%) with $I \parallel [100]$ and -0.5% (-4.0%) with $I \parallel [110]$ at 5 K. We see in Eq. (1) that the $|r_{AMR}|$ depends on the magnitudes of several parameters. Regarding the magnitude of $[D_\uparrow^{(d)} - D_\downarrow^{(d)}]$, it is approximately 4 times larger for Ni_3FeN than $NiFe_3N$ from first-principle calculations.[21] We therefore may state that larger $|r_{AMR}|$ for Ni_3FeN than $NiFe_3N$ comes from larger magnitude of $[D_\uparrow^{(d)} - D_\downarrow^{(d)}]$ for Ni_3FeN than $NiFe_3N$ in this regard. However, other parameters such as $(\sigma_\uparrow - \sigma_\downarrow)$ have not been reported, making difficult to discuss the magnitude relation of $|r_{AMR}|$ between $NiFe_3N$ and Ni_3FeN. The current direction dependence of r_{AMR} can be explained by that of *s-d* scattering in the following way. The magnitude of *s-d* scattering changes with the degree of overlap of orbitals between conductive electrons and localized *d*

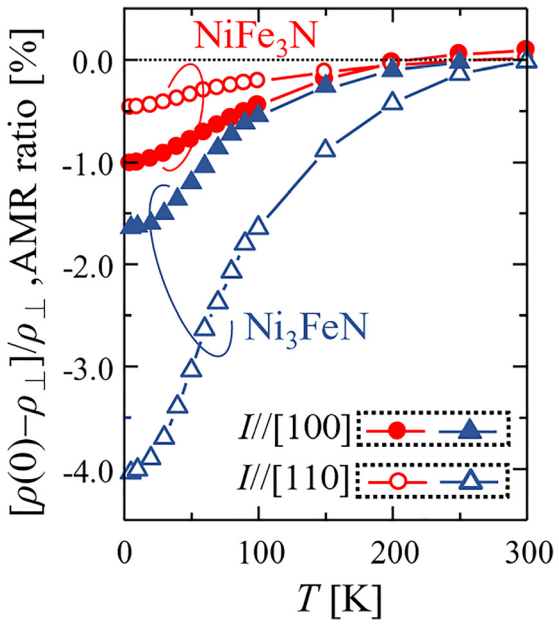

FIG. 6. Temperature dependence of r_{AMR} in the $NiFe_3N$ and Ni_3FeN films.

electrons along the current direction. According to the AMR theory taking the crystal field effect and SOI into account, the magnitude of *s*-*d* scattering is modified depending on the $D^{(d)}$ split by the crystal field effect.[9] Furthermore, the direction dependence of r_{AMR} is likely to appear because of the difference in 3*d* orbital at E_F by SOI and by crystal field along the current direction. Hence, the current direction dependence of $Ni_xFe_{4-x}N$ ($x=1$ and 3) arises from the difference of 3*d* orbitals deformation at E_F in the *s*-*d* scattering between $I \parallel [100]$ and [110].

Figure 7 shows the Fourier coefficients of the AMR curves obtained for (a) $NiFe_3N$ and (b) Ni_3FeN by fitting least-means-square-method with

$$\frac{\rho(\phi)-\rho_\perp}{\rho_\perp} = C_0 + C_2\cos 2\phi + C_4\cos 4\phi, \tag{2}$$

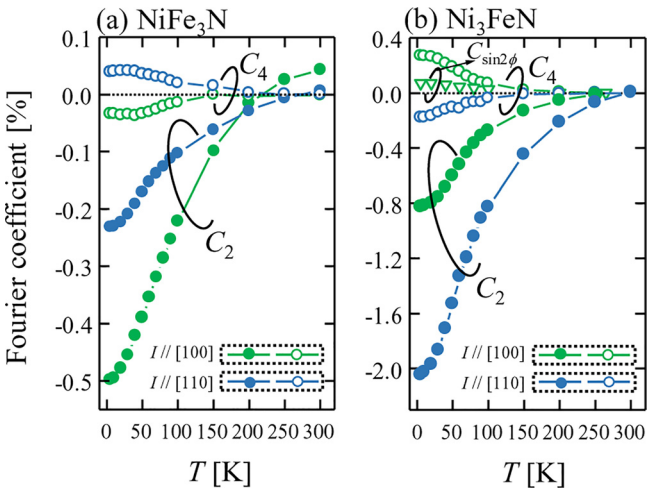

FIG. 7. Fourier coefficients of $\cos 2\phi$ (C_2), $\cos 4\phi$ (C_4), and $\sin 2\phi$ ($C_{\sin 2\phi}$) terms in the $[\rho(\phi)-\rho_\perp]/\rho_\perp$ curves for (a)$NiFe_3N$ and (b)Ni_3FeN films as a function of temperature.

where C_0 ($=C_2-C_4$) is a constant, and C_2 and C_4 are the Fourier coefficients of the $\cos 2\phi$ and $\cos 4\phi$ components, respectively. The r_{AMR} corresponds to $2C_2$. Equation (2) can be derived from the following phenomenological expression in single crystalline cubic ferromagnets by Döring as:[24,27]

$$\begin{aligned}\frac{\Delta\rho}{\rho} &= k_1\left(\alpha_1^2\beta_1^2+\alpha_2^2\beta_2^2+\alpha_3^2\beta_3^2-\frac{1}{3}\right)\\ &+2k_2(\alpha_1\alpha_2\beta_1\beta_2+\alpha_2\alpha_3\beta_2\beta_3+\alpha_3\alpha_1\beta_3\beta_1)+k_3\left(s-\frac{1}{3}\right)\\ &+k_4\left(\alpha_1^4\beta_1^2+\alpha_2^4\beta_2^2+\alpha_3^4\beta_3^2+\frac{2}{3}s-\frac{1}{3}\right)\\ &+2k_5\left(\alpha_1\alpha_2\alpha_3^2\beta_1\beta_2+\alpha_2\alpha_3\alpha_1^2\beta_2\beta_3+\alpha_3\alpha_1\alpha_2^2\beta_3\beta_1\right),\end{aligned} \tag{3}$$

where $s=\alpha_1^2\alpha_2^2+\alpha_2^2\alpha_3^2+\alpha_3^2\alpha_1^2$ and k_i is the magnetoresistance constant, which determines the temperature dependence of the AMR effect. α_j and β_j are the direction cosines of *M* and *I*, respectively. When *M* rotates in the film plane with respect to *I* flowing in the [100] ([110]) direction, $\alpha_1=\cos\phi$, $\alpha_2=\sin\phi$, $\alpha_3=0$, $\beta_1=1$ ($\beta_1=\sqrt{2}/2$), $\beta_2=0$ ($\beta_2=\sqrt{2}/2$) and $\beta_3=0$ ($\beta_3=0$). Substituting these values into Eq. (3), the angular dependence of resistivity normalized by $\rho_\perp$ is expressed as Eq. (2). Here, we added the $\sin 2\phi$ component to Eq. (2) to fit the AMR curve in case of Ni_3FeN with $I \parallel [100]$, because it was deviated from the cosine function as mentioned before. This can be explained as follows. If the direction of the Ni_3FeN stripe is displaced by a small angle δ with respect to the [100] direction on the sample surface, the direction cosine of *I* will be altered to $\beta_1=1-\delta^2/2$, $\beta_2=\delta$, and $\beta_3=0$. Using these values in Eq. (3) and considering up to the δ^2 term, Eq. (2) is modified as

$$\begin{aligned}\frac{\rho(\phi)-\rho_\perp}{\rho_\perp} &= \left(\frac{1}{6}k_1-\frac{5}{24}k_3+\frac{1}{8}k_4\right)+k_2\delta\sin 2\phi\\ &+\left(\frac{1}{2}-\delta^2\right)(k_1+k_4)\cos 2\phi\\ &+\left(-\frac{1}{8}k_3+\frac{1}{24}k_4\right)\cos 4\phi.\end{aligned} \tag{4}$$

Thus, the sine component ($k_2\delta = C_{\sin 2\phi}$) appears. It can be presumed that the deviation from the cosine function is attributed to the displacement of the stripe from the planned direction. The sine component was necessary only for Ni_3FeN to fit the experimental result probably because the k_2 of Ni_3FeN is much larger than other materials such as $NiFe_3N$ and Fe_4N. $C_{\sin 2\phi}$ was decreased as the increase of temperature and became almost 0 above 200 K as shown in Fig. 7(b). The AMR curves were mostly reproduced by C_2 above 100 K; however, C_4 appeared below 100 K. These behaviors are similar to that in Fe_4N below 50 K.[10–15] That the C_4's for $I \parallel [100]$ and [110] have the same magnitude but the opposite sign for both $NiFe_3N$ and Ni_3FeN, is easily understood from Eq. (3) by calculating C_4 in the respective current directions ($C_4^{[100]}=-C_4^{[110]}$).[11]

We next move on to the discussion about the temperature dependence of C_2 and C_4. The quantities C_2 and C_4

depend on $D^{(d)}$ split by the crystal field effect.[9] The sign of C_2 in the case of $I \parallel [100]$ is determined by the sign of $[D_\gamma - D_\varepsilon]$, where D_γ (D_ε) is the partial D of the d_γ (d_ε) orbitals at E_F. The sign change of C_2 in Fig. 7(a) can be explained by that of $[D_\gamma - D_\varepsilon]$. Moreover, when the tetragonal crystal field is enhanced, the d_ε orbital is split further into $d_{\varepsilon+}$ and $d_{\varepsilon 0}$; thus, the C_4 term appears.[9] A sharp increase in the C_4 contribution below 100 K is probably caused by the enhancement of the crystal field effect in the tetragonal symmetry. According to the previous report on Fe_4N,[28] wherein C_4 changed sharply below 50 K, the origin of tetragonal crystal field is considered to be caused by the change in the magnetic structure. The change of crystal structure was not detected even below 50 K. We therefore speculate that similar transformation of the magnetic symmetry occurs also in $Ni_xFe_{4-x}N$ ($x = 1$ and 3) below 100 K. However, we have limited information to discuss further at present. Thus, further theoretical and experimental investigations are required to explain the temperature and direction dependences of C_2 and C_4 in more detail and get to the origin of C_4.

IV. CONCLUSION

We measured the AMR effect of $Ni_xFe_{4-x}N$ ($x = 1$ and 3) epitaxial films grown on the STO(001) single-crystal substrate and investigated their magnetotransport properties. Negative AMR effect was observed at almost all the measured temperatures. It became clear that the minority spin transport is dominant in $Ni_xFe_{4-x}N$ ($x = 1$ and 3), similar to those in Fe_4N and Co_3FeN, at least in the temperature range of negative AMR effect. In the case of Ni_3FeN, $|r_{AMR}|$ became almost 0 at 260 K and this temperature well agreed with T_c, determined from the temperature dependence of magnetization. $|r_{AMR}|$ was gradually increased with decreasing temperature and significantly increased below 100 K. The AMR curves were reproduced well by using the $\cos 2\phi$ component above 100 K, but the contribution of $\cos 4\phi$ term became pronounced below 100 K. It is assumed that the tetragonal crystal field was enhanced at low temperature.

ACKNOWLEDGMENTS

The authors acknowledge Mr. T. Gushi, S. Higashikozono, and Dr. K. Toko for their help, discussions, and encouragements to pursue this work. This work was financially supported in part by JSPS Grants-in-Aid for Scientific Research (A) (No. 26249037), JSPS Fellows (No. 14J01804), the cooperative research projects (H26/A04) from the Research Institute of Electric Communication, Tohoku University, and the cooperative research projects from the Center for Spintronics Research Network, Tohoku University.

[1] S. Kokado, N. Fujita, K. Harigaya, H. Shimizu, and A. Sakuma, Phys. Rev. B **73**, 172410 (2006).
[2] A. Narahara, K. Ito, T. Suemasu, Y. K. Takahashi, A. Ranajikanth, and K. Hono, Appl. Phys. Lett. **94**, 202502 (2009).
[3] Y. Komasaki, M. Tsunoda, S. Isogami, C.-C. Chen, and M. Takahashi, J. Magn. Soc. Jpn. **34**, 524 (2010).
[4] K. Sunaga, M. Tsunoda, K. Komagaki, Y. Uehara, and M. Takahashi, J. Appl. Phys. **102**, 013917 (2007).
[5] Y. Komasaki, M. Tsunoda, S. Isogami, and M. Takahashi, J. Appl. Phys. **105**, 07C928 (2009).
[6] S. Isogami, M. Tsunoda, Y. Komasaki, A. Sakuma, and M. Takahashi, Appl. Phys. Express **3**, 103002 (2010).
[7] S. Kokado, M. Tsunoda, K. Harigaya, and A. Sakuma, J. Phys. Soc. Jpn. **81**, 024705 (2012).
[8] S. Kokado and M. Tsunoda, Adv. Mater. Res. **750–752**, 978 (2013).
[9] S. Kokado and M. Tsunoda, J. Phys. Soc. Jpn. **84**, 094710 (2015).
[10] M. Tsunoda, Y. Komasaki, S. Kokado, S. Isogami, C.-C. Chen, and M. Takahashi, Appl. Phys. Express **2**, 083001 (2009).
[11] M. Tsunoda, H. Takahashi, S. Kokado, Y. Komasaki, A. Sakuma, and M. Takahashi, Appl. Phys. Express **3**, 113003 (2010).
[12] K. Ito, K. Kabara, H. Takahashi, T. Sanai, K. Toko, T. Suemasu, and M. Tsunoda, Jpn. J. Appl. Phys. **51**, 068001 (2012).
[13] K. Kabara, M. Tsunoda, and S. Kokado, Appl. Phys. Express **7**, 063003 (2014).
[14] K. Ito, K. Kabara, T. Sanai, K. Toko, Y. Imai, M. Tsunoda, and T. Suemasu, J. Appl. Phys. **116**, 053912 (2014).
[15] Z. R. Li, X. P. Feng, X. C. Wang, and W. B. Mi, Mater. Res. Bull. **65**, 175 (2015).
[16] F. J. Yang, Y. Sakuraba, S. Kokado, Y. Kota, A. Sakuma, and K. Takanashi, Phys. Rev. B **86**, 020409(R) (2012).
[17] Y. Sakuraba, S. Kokado, Y. Hirayama, T. Furubayashi, H. Sukegawa, S. Li, Y. K. Takahashi, and K. Hono, Appl. Phys. Lett. **104**, 172407 (2014).
[18] K. Srinivas, M. Mannivel Raja, S. Arumugam, and S. V. Kamat, Physica B **448**, 167 (2014).
[19] Y. Du, G. Z. Xu, E. K. Liu, G. J. Li, H. G. Zhang, S. Y. Yu, W. H. Wang, and G. H. Wu, J. Magn. Magn. Mater. **335**, 101 (2013).
[20] K. Kabara, M. Tsunoda, and S. Kokado, AIP Adv. **6**, 055818 (2016).
[21] F. Takata, K. Ito, S. Higashikozono, T. Gushi, K. Toko, and T. Suemasu, J. Appl. Phys. **120**, 083907 (2016).
[22] R. Loloee, J. Appl. Phys. **112**, 023902 (2012).
[23] K. Kabara and M. Tsunoda, J. Appl. Phys. **117**, 17B512 (2015).
[24] R. M. Bozorth, *Ferromagnetism* (D. van Nostrand, New York, 1951).
[25] R. M. Bozorth, Phys. Rev. **70**, 923 (1946).
[26] H. C. van Elst, Physica **25**, 708 (1959).
[27] W. Döring, Ann. Phys. (Leipzig) **424**, 259 (1938).
[28] M. Tsunoda, K. Kabara, and S. Kokado, Magnetics Jpn. **11**, 125 (2016) (in Japanese).